

# RIMS analysis of ion induced fragmentation of molecules sputtered from an enriched $U_3O_8$ matrix

David Willingham · Michael R. Savina ·  
Kim B. Knight · Michael J. Pellin · Ian D. Hutcheon

Received: 15 July 2012  
© Akadémiai Kiadó, Budapest, Hungary 2012

**Abstract** Resonance ionization mass spectrometry was used to measure the composition of the sputtered flux from 15 keV  $Ga^+$ ,  $Au^+$ ,  $Au_2^+$  and  $Au_3^+$  primary ions impacting a  $^{235}U$  enriched  $U_3O_8$  standard. We demonstrate that molecular fragmentation decreases as the primary ion mass and nuclearity increases. Stopping and range of ions in matter calculations show that cluster ions ( $Au_2^+$  and  $Au_3^+$ ) deposit more of their energy via direct knock-ons with near-surface target atoms, whereas monatomic ions ( $Ga^+$  and  $Au^+$ ) penetrate much deeper into the target sub-surface region. We correlate these results to the experimental observations by showing that increased cluster ion sputter yields partition the projectile energy over a larger number of sputtered molecules. Therefore, while cluster ions deposit more total energy into the near surface region of the target compared to monatomic ions, the energy per molecule decreases with projectile mass and nuclearity. Less energy per molecule decreases the number of U–O bond breaks and, consequently, leads to a decrease in molecular fragmentation. Additionally, the extent of molecular fragmentation as a function of ion dose was evaluated. We show that molecular fragmentation increases with increased ion dose; primarily as a result of sub-surface chemical damage accumulation. The relative intensity of this effect appears to be projectile independent.

**Keywords** Resonance ionization · Mass spectrometry · Uranium · Cluster ions · Useful yield

## Introduction

The increasing threat of nuclear weapons development has prompted the use of a number of mass spectrometry techniques charged with the task of determining the isotopic composition of trace amounts of radionuclides from a diverse set of materials [1–11]. A major focus for these types of measurements is on improving the sensitivity for the detection of uranium and transuranic isotopes in the presence of isobaric interferences without the need for complex and time-consuming sample preparation methods. Recently, secondary ion mass spectrometry (SIMS) has shown promise as an effective tool for the analysis of nuclear materials with high sensitivity and minimal sample preparation [12–15]. The sensitivity of SIMS is often defined by useful yield: the number of ions detected over the number of atoms removed during the analysis. SIMS analysis of  $U_3O_8$  standards has achieved useful yields of 1–2 % using high mass resolution, multi-collector instruments [13].

Analytical resonance ionization mass spectrometry (RIMS) uses wavelength tunable lasers to selectively ionize atoms desorbed from solid surfaces either by ion sputtering or laser heating. The resulting sputtered flux is composed of secondary ions and neutrals characteristic of the sample surface chemistry. In our RIMS instruments, the ion component of the sputtered flux is suppressed electrostatically prior to photoionization of the sputtered neutrals. The neutral atoms of interest are then selectively ionized using one or two lasers with wavelengths chosen to match specific atomic resonance transitions. These electronically excited atoms are ionized

---

D. Willingham (✉) · M. R. Savina · M. J. Pellin  
Argonne National Laboratory, 9700 S. Cass Avenue, Argonne,  
IL 60439, USA  
e-mail: davidgwillingham@gmail.com

K. B. Knight · I. D. Hutcheon  
Lawrence Livermore National Laboratory, P. O. Box 808,  
Livermore, CA 94551, USA

using an additional laser with a wavelength corresponding to an autoionizing resonance of the element of interest. Photoions are extracted into a time-of-flight mass spectrometer (TOF-MS) and detected using a multi-channel plate (MCP) ion detector.

Transitioning from standard samples to more complex materials can become increasingly more complicated due to the presence of isobaric interferences. While large geometry SIMS instruments have been used to analyze uranium oxide reference materials with high precision, SIMS can be hindered by mass coincidences from same-mass isotopes, hydrides and other molecular compounds [13]. RIMS achieves its selectivity spectroscopically and, therefore, is capable of overcoming these isobaric limitations. Unfortunately, it is this very selectivity that often limits the useful yield of RIMS measurements. The useful yield of RIMS experiments depends heavily on the sample being analyzed; i.e. the useful yield for U atoms from reduced U metal is significantly larger than from  $U_3O_8$ . This is primarily a result of variations in the composition of the sputtered flux. Previous work [unpublished] has shown that ion sputtering of  $U_3O_8$  produces mainly uranium oxide ( $UO_x$ ) molecules rather than U atoms. Since RIMS is only sensitive to the specific element of interest, the useful yield for U atoms from these materials is significantly reduced. We investigate several ion sputtering regimes to better understand the mechanisms that lead to projectile dependent molecular fragmentation.

## Experimental

A CRM U500 standard material was used for all analysis reported herein. The CRM U500 was composed of sintered aggregates of micrometer sized  $U_3O_8$  grains pressed into indium foil. Additionally, the CRM U500 was isotopically enriched in  $^{235}U$  to a 1:1 ratio with  $^{238}U$ . The CRM U500 standard material was mounted to a sample holder and entered into the vacuum chamber without any further sample preparation.

RIMS analyses were performed on the CHARISMA instrument at Argonne National Laboratory; described in detail elsewhere [16]. Briefly, a solid target is sputtered using a 15 keV ion beam ( $Ga^+$ ,  $Au^+$ ,  $Au_2^+$  or  $Au_3^+$ ) from a liquid metal ion source (IOG 25, Ionoptika Ltd.) and focused to a spot size of  $\sim 10 \mu m$ . Secondary ions generated from the ion bombardment are ejected using a +4 kV bias voltage. After a short, field-free duration, the secondary neutrals are intersected with three, pulsed laser beams at  $\sim 1$  mm from the sample surface. The lasers are wavelength tunable Ti:sapphire systems that have been described in detail elsewhere [16, 17]. The laser wavelengths are tuned to excite two resonance transitions and an

autoionizing state to selectively ionize neutral U atoms within the sputtered flux. The 3-color, 3-photon RIMS scheme for U atoms used herein was adapted from work by Schumann et al. [18] and is described in detail by Isselhardt and co-workers [19]. The resonantly ionized U atoms are then extracted into a reflectron-type TOF-MS at +2 kV and focused onto a MCP ion detector. Single ion event signals from the ion detector were digitized by a time-to-digital board (P7889, FAST ComTec GmbH). The resulting mass spectra are typically a summation of 10,000 individual analysis cycles acquired at a repetition rate of 1 kHz. For experiments performed at increased primary ion duty cycle, a second primary ion pulse was added to each analysis cycle ranging from 5 to 400  $\mu s$ ; permitting duty cycles as large as 40 %.

Although specifically targeted at neutral U atoms, the RIMS scheme used herein also inadvertently ionizes  $UO_x$  molecules. The photoionization of  $UO_x$  molecules originates from a  $1 + 1$  resonance enhance multi-photon ionization (REMPI) process involving the 1st resonance laser (415.511 nm) from the RIMS scheme. Despite the small photoionization cross-section for this process compared to U atoms, the laser power (150–500 mW) used in these experiments is high enough to ionize both  $UO$  and  $UO_2$  species.

## Results and discussion

The nature of ion–solid interactions is primarily governed by the efficiency of energy transfer from the primary ion to the surface and sub-surface atoms. Ion sputtering can be described by a sequence of elastic collisions between point particles [20]. In this process, the bombarding ion transfers its energy to the target atoms, thereby initiating a series of collision cascades within the near-surface region; although much of the energy of the projectile is deposited much deeper within the bulk. Collisions that recoil back through the sample surface result in sputtered material; whereas, collisions occurring at greater penetration depths lead to sub-surface chemical damage. Until recently, ion beam analysis of surfaces used only monatomic ions such as  $Ar^+$ ,  $Ga^+$  and  $In^+$ ; however, the advent of cluster ion sources has led to a paradigm shift in the way we think about ion–solid interactions. Cluster ion beams such as  $Au_3^+$ ,  $Bi_3^+$  and  $C_{60}^+$  provide  $\sim 3$  orders of magnitude increase in sputter yield as compared to monatomic ion sources [21–23]. This is because, unlike the collision cascade generated by monatomic ions, cluster ions deposit a majority of their energy within the first few nanometers of the surface. The observed cluster ion sputter yields increase non-linearly with cluster nuclearity; indicating a significant deviation from the collision cascade model.

In addition to primary ion dependent variations in sputter yield, it is possible to measure the kinetic energy distribution of sputtered material using sophisticated photoionization techniques [24–27]. These methods can provide insight into the mechanism of energy transfer from the primary ion to the surface and sub-surface atoms. The analysis of molecular solids, however, is significantly more complicated due to the partitioning of energy imparted to the sputtered molecules into various fragmentation pathways. This makes it increasingly difficult to infer specific details about the internal energy distribution of the sputtered molecules from the kinetic energy distribution. The complexity of the mass spectra obtained from molecular solids, however, can be used to our advantage in this situation. The mass spectra of molecular species often contain parent mass peaks ( $\text{UO}_2$  and  $\text{UO}$  molecules) and fragment mass peaks ( $\text{U}$  atoms). The extent of fragmentation can be determined simply by taking the ratio of ion counts in the parent mass over the ion counts in the fragment masses ( $M/F$ ). Previous work has indicated that the  $M/F$  of poly-aromatic hydrocarbons (PAHs) as well as the specific fragmentation pathway (carbon loss compared to hydrogen loss) can be correlated to the average internal energy of the sputtered flux [28, 29].

Variations in the extent of fragmentation of sputtered molecules are known to be projectile dependent. Cluster ion sputtering of polymers has been shown to increase the probability of direct impacts (or knock-ons) with target atoms compared to monatomic ions resulting in ejection of predominantly molecular fragments [30, 31]. In contrast, previous work comparing the sputtering of PAHs with  $\text{Au}^+$  and  $\text{C}_{60}^+$  showed that molecular fragmentation was reduced with cluster ion sputtering [29]. It is clear that the extent of molecular fragmentation in any system is heavily dependent on the material being analyzed as well as the nuclearity and mass of the primary ion probe. The efforts described herein focus on ion sputtering of  $\text{U}_3\text{O}_8$  with a number of different primary ions ( $\text{Ga}^+$ ,  $\text{Au}^+$ ,  $\text{Au}_2^+$ ,  $\text{Au}_3^+$ ). By comparing the ratio of the parent mass to the fragment mass ions as a function of primary ion mass and nuclearity, we aim to determine the effects of cluster ion sputtering on the useful yield of  $\text{U}$  atoms from  $\text{U}_3\text{O}_8$ .

Mass spectra are shown in Fig. 1. Peaks correspond to resonantly ionized  $\text{U}$  atoms and  $\text{UO}_x$  molecules ionized via a  $1 + 1$  REMPI process. Photoionization cross-sections for each of these species have been calculated previously [unpublished] using the saturation ionization technique [32]. This technique allows for direct conversion of the observed ion signals into the composition of the sputtered flux. The data in Table 1 illustrates the need to adjust each ion signal according to its cross-section in order to obtain the correct  $M/F$  ratios and percent compositions of  $\text{U}$  atoms in the sputter flux. The  $M/F$  ratios in each case consider the  $\text{UO}_2$  and  $\text{UO}$

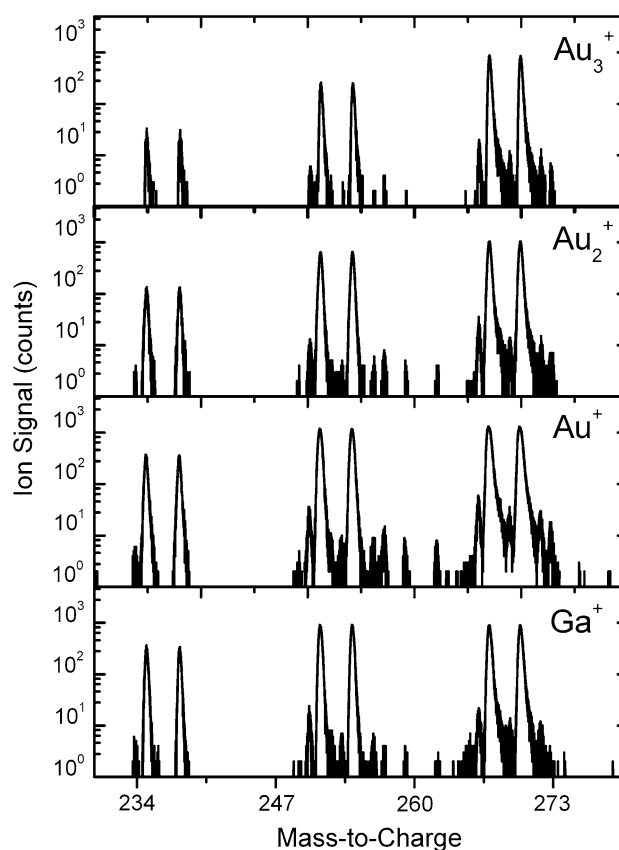


**Fig. 1** Mass spectra obtained by ion sputtering of  $\text{U}_3\text{O}_8$  with 15 keV  $\text{Au}_3^+$ ,  $\text{Au}_2^+$ ,  $\text{Au}^+$  and  $\text{Ga}^+$ . Characteristic mass peaks include  $^{235}\text{U}^+$ ,  $^{238}\text{U}^+$ ,  $^{235}\text{U}^{16}\text{O}^+$ ,  $^{238}\text{U}^{16}\text{O}^+$ ,  $^{235}\text{U}^{16}\text{O}_2^+$  and  $^{238}\text{U}^{16}\text{O}_2^+$

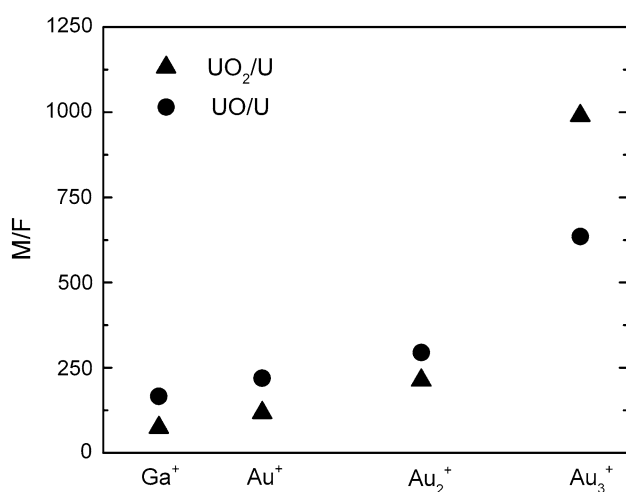
molecules as two separate parent masses with  $\text{U}$  atoms as the fragment mass. This treatment of the data is used for simplicity and does not include the full complement of known fragmentation pathways for gas phase  $\text{UO}_x$  molecules [33].

The  $M/F$  ratios ( $\text{UO}_2/\text{U}$  and  $\text{UO}/\text{U}$ ) for each primary ion as a function of its mass are shown in Fig. 2. Clearly, the  $M/F$  increases and, therefore, the extent of fragmentation of  $\text{UO}_x$  molecules to  $\text{U}$  atoms decreases with increased mass of the primary ion. In addition, this decreased fragmentation is enhanced non-linearly as a function of primary ion nuclearity; i.e. the  $M/F$  ratio ( $\text{UO}_2/\text{U}$ ) from  $\text{Au}_3^+$  bombardment is  $8.5 \times$  larger than that of  $\text{Au}^+$ , which has  $1/3$  the mass. These results can be investigated further using Monte-Carlo computational modeling methods [34]. The stopping and range of ions in matter (SRIM) 2011 software was used to model the ion-atom collisions of  $\text{U}_3\text{O}_8$  with  $\text{Ga}^+$ ,  $\text{Au}^+$ ,  $\text{Au}_2^+$  and  $\text{Au}_3^+$ . This computational approach deviates from our experimental setup in two significant aspects. First, the model contains a stoichiometric arrangement of  $\text{U}$  and  $\text{O}$  atoms with the density and surface binding energy of  $\text{U}_3\text{O}_8$ , but without treatment of chemical bonding configurations. Secondly, SRIM only models monatomic primary ions; therefore, the cluster ions

**Table 1** Conversion of the experimentally measured ion signals to the actual number of sputtered neutrals within the laser volume using the saturation ionization technique

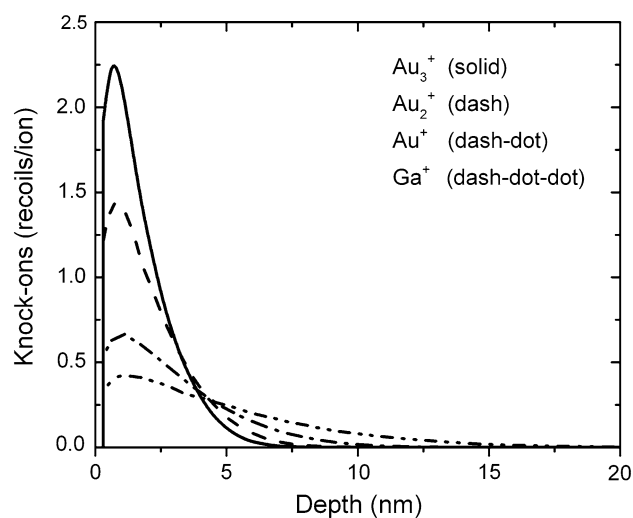
	$\sigma$ (cm <sup>2</sup> )	Ion signals				Sputtered neutrals			
		Ga <sup>+</sup>	Au <sup>+</sup>	Au <sub>2</sub> <sup>+</sup>	Au <sub>3</sub> <sup>+</sup>	Ga <sup>+</sup>	Au <sup>+</sup>	Au <sub>2</sub> <sup>+</sup>	Au <sub>3</sub> <sup>+</sup>
U	$2.1 \times 10^{-15}$	30,628	35,972	11,770	1,709	30,692	36,047	11,794	1,713
UO	$2.0 \times 10^{-22}$	96,698	149,976	66,064	20,657	508,934	789,344	347,704	108,721
UO <sub>2</sub>	$3.0 \times 10^{-23}$	110,194	203,899	120,721	81,364	229,570	424,788	251,501	169,508
UO/U		3.16	4.17	5.61	12.09	165.82	218.98	294.80	634.84
UO <sub>2</sub> /U		3.60	5.67	10.26	47.61	74.80	117.84	213.24	989.80
% Composition of uranium atoms						0.42	0.30	0.20	0.06

Photoionization cross-sections ( $\sigma$ ) for U, UO and UO<sub>2</sub> neutrals are listed. The M/F ratios using UO<sup>+</sup> and UO<sub>2</sub><sup>+</sup> as parent ions and U<sup>+</sup> as the fragment ion are shown for each primary ion using the ion signals and the calculated number of sputtered neutrals. The percentage of U atoms in the sputtered flux for each primary ion is indicated

**Fig. 2** M/F ratios for Ga<sup>+</sup>, Au<sup>+</sup>, Au<sub>2</sub><sup>+</sup> and Au<sub>3</sub><sup>+</sup> where the parent mass is either UO<sub>2</sub> (triangles) or UO (circles) and the fragment mass is always U

were approximated by running the simulation at monoatomic kinetic energies reduced by the cluster nuclearity; i.e. 15 keV Au<sub>2</sub><sup>+</sup> and Au<sub>3</sub><sup>+</sup> were approximated by Au<sup>+</sup> at 7.5 and 5 keV respectively. This method for approximating cluster ion sputtering has been shown to be valid for materials with large sublimation energies where the non-linear sputter yield enhancements are small [35]. Although it is not possible to make a direct comparison to the experimental results, the data provided by the SRIM calculation provides valuable insight into the mechanism of energy transfer between the primary ion and the target atoms.

The data in Fig. 3 from the SRIM simulations show the number of direct knock-ons of the primary ion with target atoms as a function of depth from the surface. Here we can see that the total number of knock-ons increases as a function of primary ion mass and nuclearity allowing for more direct transfer of energy from the primary ion to the

**Fig. 3** SRIM calculations of the number of direct knock-ons of Au<sub>3</sub><sup>+</sup> (solid), Au<sub>2</sub><sup>+</sup> (dash), Au<sup>+</sup> (dash-dot) and Ga<sup>+</sup> (dash-dot-dot) with U<sub>3</sub>O<sub>8</sub> target atoms as a function of sample depth

target atoms. Additionally, the sampling depth of these knock-ons becomes shallower with increasing primary ion mass and nuclearity, indicating that cluster ions deposit energy much closer to the sample surface than monoatomic ions.

Figure 4 shows that although the total energy imparted to the sputtered flux increases, the energy per secondary species decreases with increasing primary ion mass and nuclearity. This observation provides a direct correlation between the experimental measurements and the computational model. As the primary ion mass and nuclearity increases, the probability of direct knock-ons with the target atoms increases and more energy is imparted from the primary ion to the target atoms. However, because the sputter yield increases as well, the total energy imparted from the primary ion is partitioned over a much larger sputtered flux causing the energy per secondary species to

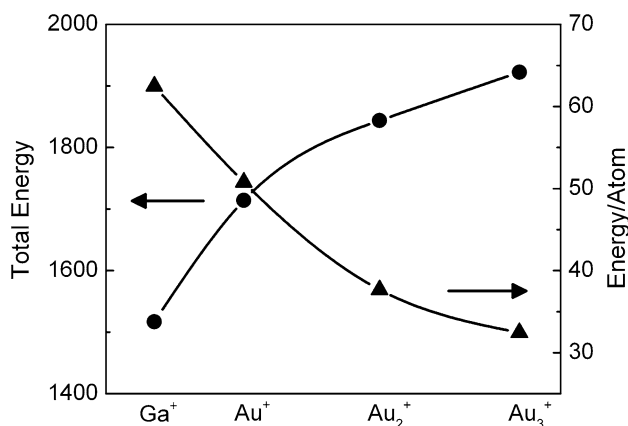


**Fig. 4** SRIM calculations of the total energy (eV) of the sputtered flux (circles) versus the energy (eV) per sputtered atom (triangles) for Ga<sup>+</sup>, Au<sup>+</sup>, Au<sub>2</sub><sup>+</sup> and Au<sub>3</sub><sup>+</sup>. The left and right axes indicated by the arrows are associated with the circles and triangles respectively. The lines through the data points are to guide the eye and do not represent a fit to the data

decrease. Less energy per secondary species means less energy available to break U–O bonds and, therefore, less fragmentation of UO<sub>x</sub> molecules. This computational result corroborates the experimental data showing increased M/F ratios as a function of increased primary ion mass and nuclearity. Although not a true quantitative argument, qualitatively the experimental and computational trends show significant agreement.

In addition to the energy distribution of the sputtered flux, the build-up of sub-surface chemical damage is known to increase the amount of molecular fragmentation observed during subsequent analyses [36–39]. This result has primarily been observed under dynamic sputtering conditions, but can be replicated for pulsed analysis by increasing the primary ion duty cycle. In a typical RIMS experiment, the primary ion pulse lasts for 300–500 ns. After ~250 μs, all of the U<sup>+</sup> and UO<sub>x</sub><sup>+</sup> ions have traversed the flight tube and have reached the detector. At a repetition rate of 1 kHz, this means that there is a 750 μs wait until the next ion pulse starts the subsequent analysis. During this time, the ion gun can be operated continuously to increase the primary ion duty cycle of each analysis cycle to a maximum of 50 %; this limit is imposed by our high voltage power supplies, not by the available time window.

Figure 5 illustrates the dependence of UO<sub>2</sub>/U as a function of primary ion dose for Au<sup>+</sup>, Au<sub>2</sub><sup>+</sup> and Au<sub>3</sub><sup>+</sup>. From this data we see that the extent of fragmentation increases with increased primary ion dose. This is primarily a result of chemical damage build-up by the continuous sputtering portion of each analysis cycle. The observed behavior can be fit to the following equation:

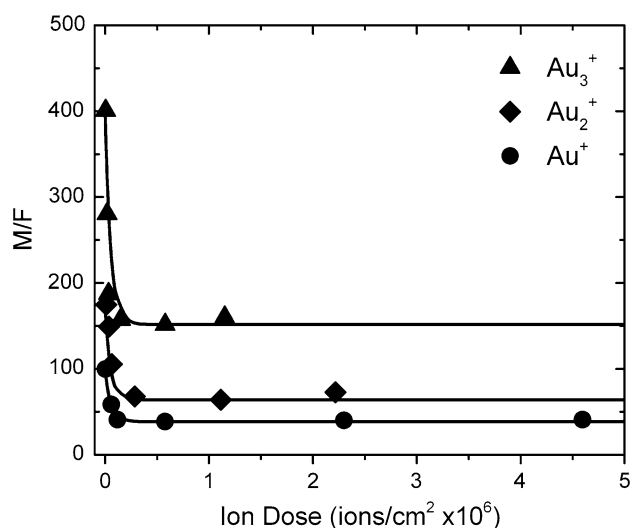


**Fig. 5** M/F ratios for Au<sub>3</sub><sup>+</sup> (triangles), Au<sub>2</sub><sup>+</sup> (diamonds) and Au<sup>+</sup> (circles) versus primary ion dose. Solid lines indicate the least squares fit of each data set to Eq. 1

$$\gamma = \gamma_{ss} + (\gamma_0 - \gamma_{ss}) \exp(-\sigma_f f) \quad (1)$$

where  $\gamma$  is the measured UO<sub>2</sub>/U with  $\gamma_0$ , and  $\gamma_{ss}$  being the initial (designated by the minimum ion dose) and steady-state (the point at which increased ion dose does not decrease the UO<sub>2</sub>/U further) values, respectively,  $\sigma_f$  (cm<sup>2</sup>) is the fragmentation cross-section and  $f$  is the primary ion fluence (ions/cm<sup>2</sup>). The fragmentation cross-sections were determined to be  $1.98 \times 10^{-5}$  cm<sup>2</sup>,  $2.08 \times 10^{-5}$  cm<sup>2</sup> and  $1.92 \times 10^{-5}$  cm<sup>2</sup> for Au<sup>+</sup>, Au<sub>2</sub><sup>+</sup> and Au<sub>3</sub><sup>+</sup> respectively. We speculate that these data result from a convolution of projectile dependent molecular fragmentation and ion-induced preferential sputtering of oxygen from the U<sub>3</sub>O<sub>8</sub> matrix at high ion doses [40]. Therefore, as the surface becomes chemically reduced, the amount of U atoms in the sputtered flux, which is indicative of the surface composition, increases with increased ion dose. The number of U atoms in the sputtered flux is further increased by projectile dependent molecular fragmentation from the subsequent analysis beam. In our experiment, the analysis beam and the reducing beam are the same projectile operated under different sputter conditions. We plan to verify our hypothesis by experiments where the analysis beam and the reducing beam are decoupled from one another. Unfortunately, a direct correlation between M/F and useful yield cannot be made because the ions generated during the dynamic portion of the analysis are not being detected. However, it is likely that this observation accounts for some of the discrepancy in useful yield measurement observed between pulsed RIMS experiments and dynamic SIMS experiments.

## Conclusion

The primary ion dependence of fragmentation of  $\text{UO}_x$  molecules has been investigated. The results show that molecular fragmentation is decreased as the mass and nuclearity of the primary ion increases. SRIM calculations show that cluster ions deposit the majority of their energy closer to the target surface than monatomic ions. Although the transfer of energy from the cluster ions to the target atoms is more efficient, increased sputter yields partition the primary ion energy over a larger number of ejected species, resulting in less energy per sputtered molecule. Lowering the energy per molecule as a function of primary ion mass and nuclearity decreases the probability of molecular fragmentation and is characterized by the increased M/F ratios observed experimentally. In addition, the extent of molecular fragmentation as a function of ion dose was evaluated for several primary ions. Molecular fragmentation increases as the ion dose increases, and the relative amount of increase is projectile independent. These data suggest that sub-surface chemical damage caused by ion sputtering results in more U atoms in the sputtered flux of subsequent ion impacts. It is likely that RIMS measurements taken at higher ion doses will result in an increased useful yield of U atoms from  $\text{U}_3\text{O}_8$  matrices.

**Acknowledgments** The sputtering experiments and SRIM calculations were supported by the U.S. Department of Energy, Office of Basic Energy Sciences, Division of Material Sciences and Engineering under award number DEAC02-06CH11357 (D.G.W., M.R.S., and M.J.P.). Sample preparation and assistance with some of the sputtering experiments was supported under the auspices of the U.S. Department of Energy by Lawrence Livermore National Laboratory under Contract DE-AC52-07NA27344 (K.B.K. and I.D.H.) through Laboratory Directed Research and Development Program at LLNL (project 10-SI-016), as well as with support from the Department of Energy Office of Nonproliferation Research and Development and the U.S. Department of Homeland Security, LLNL-JRNL-551175.

## References

- Bürger S, Riciputi LR, Bostick DA, Turgeon S, McBay EH, Lavelle M (2009) *Int J Mass Spectrom* 286:70
- Betti M, Tamborini G, Koch L (1999) *Anal Chem* 71:2616
- Günther-Leopold I, Waldis JK, Wernli B, Kopajtic Z (2005) *Int J Mass Spectrom* 242:197
- Kraiem M, Richter S, Kulhn H, Stefaniak EA, Kerckhove G, Truyens J, Aregbe Y (2011) *Anal Chem* 83:3011
- Pitois AL, de Heras Las L, Betti M (2008) *Int J Mass Spectrom* 273:95
- Tamborini G, Betti M, Forcina V, Hiernaut T, Giovannone B, Koch L (1998) *Spectrochim Acta* 53:1289
- Zhang XZ, Esaka F, Esaka KT, Magara M, Sakurai S, Usuda S, Watanabe K (2007) *Spectrochim Acta* 62:1130
- Esaka F, Magara M, Lee CG, Sakurai S, Usuda S, Shinohara N (2009) *Talanta* 78:290–294
- Pointurier F, Pottin AC, Hemet P, Hubert A (2011) *Spectrochimica Acta* 66:261–267
- Pointurier F, Pottin AC, Hubert A (2011) *Anal Chem* 83:7841–7848
- Szeles E, Varga Z, Stefanka Z (2010) *J Anal At Spectrom* 25:1014–1018
- Allen GC, Brown IT, Harris SJ (1994) *Beam Interact Mater Atoms* 88:170–173
- Ranebo Y, Hedberg PML, Whitehouse MJ, Ingeneri K, Littmann S (2009) *J Anal At Spectrom* 24:277–287
- Hedberg PML, Peres P, Cliff JB, Rabemananjara F, Littmann S, Thiele H, Vincent C, Albert N (2011) *J Anal At Spectrom* 26:406
- Ranebo Y, Niagolova N, Erdmann N, Eriksson M, Tamborini G, Betti M (2010) *Anal Chem* 82:4055–4062
- Savina MR, Pellin MJ, Tripa CE, Veryovkin IV, Calaway WF, Davis AM (2003) *Geochim Cosmochim Acta* 67:3215–3225
- Levine J, Savina MR, Stephan T, Dauphas N, Davis AM, Knight KB, Pellin MJ (2009) *Int J Mass Spectrom* 288:36–43
- Schumann PG, Wendt kDa, Bushaw BA (2005) *Spectrochimica Acta* 60:1402–1411
- Isselhardt BH, Savina MR, Knight KB, Pellin MJ, Hutcheon ID, Prussin SG (2011) *Anal Chem* 83:2469–2475
- Andersen HH, Sigmund P (1965) *Phys Lett* 15:237
- Davies N, Weibel DE, Blenkinsopp P, Lockyer N, Hill R, Vickerman JC (2003) *Appl Surf Sci* 203:223–227
- Touboul D, Kollmer F, Niehuis E, Brunelle A, Laprevote O (2005) *J Am Soc Mass Spectrom* 16:1608–1618
- Ryan KE, Wojciechowski IA, Garrison BJ (2007) *J Phys Chem C* 111:12822–12826
- Brenes DA, Garrison BJ, Winograd N, Postawa Z, Wucher A, Blenkinsopp P (2011) *J Phys Chem Lett* 2:2009–2014
- Brenes DA, Willingham D, Winograd N, Postawa Z (2011) *Surf Interface Anal* 43:78
- Coon SR, Calaway WF, Burnett JW, Pellin MJ, Gruen DM, Spiegel DR, White JM (1991) *Surf Sci* 259:275
- Coon SR, Calaway WF, Pellin MJ, Curlee GA, White JM (1993) *Beam Interact Mater Atoms* 82:329–336
- Kuhlewind H, Kiermeier A, Neusser HJ (1986) *J Chem Phys* 85:4427
- Willingham D, Kucher A, Winograd N (2008) *Appl Surf Sci* 255:831–833
- Czerwinski B, Samson R, Garrison BJ, Winograd N, Postawa Z (2006) *Vacuum* 81:167–173
- Kotter F, Benninghoven A (1998) *Appl Surf Sci* 133:47–57
- Ambartzumian R, Furzikov N, Letokhov V, Puretsky A (1976) *Appl Phys A Mater Sci Process* 9:335
- Capone F, Colle Y, Hiernaut JP, Ronchi C (1999) *J Phys Chem A* 103:10899–10906
- Ziegler JF, Ziegler MD, Biersack JP (2010) *Beam Interact Mater Atoms* 268:1818–1823
- Poerschke D, Wucher A (2011) *Surf Interface Anal* 43:171–174
- Willingham D, Brenes DA, Winograd N, Wucher A (2011) *Surf Interface Anal* 43:45
- Willingham D, Brenes DA, Wucher A, Winograd N (2010) *J Phys Chem C* 114:5391–5399
- Cheng J, Winograd N (2005) *Anal Chem* 77:3651–3659
- Wucher A (2008) *Surf Interface Anal* 40:1545–1551
- Idriss H, Senanayake SD, Waterhouse GIN, Chan ASY, Madey TE, Mullins DR (2007) *J Phys Chem C* 111:7963–7970